RSC Advances

Synthesis of Cu@Fe3O4 nanowire electrode for Li-ion batteries

Journal:	*RSC Advances*
Manuscript ID:	RA-ART-07-2014-007496.R1
Article Type:	Paper
Date Submitted by the Author:	27-Aug-2014
Complete List of Authors:	Han, Bing; Kunming University of Science and Technology, College of Materials Science and Engineering Zhang, Shichao; Beihang University, School of Materials Science and Engineering Zhou, Rong; Kunming University of Science and Technology, College of Materials Science and Engineering Wu, Xiaomeng; Beihang University, School of Materials Science and Engineering Wei, Xin; Beihang University, School of Materials Science and Engineering Xing, Yalan; Beihang University, School of Materials Science and Engineering Wang, Shengbin; Beihang University, School of Materials Science and Engineering Qi, Tao; Beihang University, School of Materials Science and Engineering

Cite this: DOI: 10.1039/c0xx00000x

www.rsc.org/xxxxxx

ARTICLE TYPE

Synthesis of Cu@Fe$_3$O$_4$ Nanowire Arrays Electrode for Li-ion batteries

Bing Han[a], Shichao Zhang[*,b] ,Rong Zhou[a], Xiaomeng Wu[b] ,Xin Wei[b], Yalan Xing[b], Shengbin Wang[b] and Tao Qi[b]

Received (in XXX, XXX) Xth XXXXXXXXX 20XX, Accepted Xth XXXXXXXXX 20XX

DOI: 10.1039/b000000x

Three-dimensional (3D) electrodes of Cu@Fe$_3$O$_4$ nanowrie arrays for Li-ion batteries are prepared by electrochemical route. The XRD, SEM, TEM and HRTEM are used to characterize the micromorphology. The structures are improved, which is beneficial for the electrochemical performances. The obtained electrodes show a higher initial capacity than the traditional Cu@Fe$_3$O$_4$ planar electrodes. Moreover, the 3D electrodes exhibit better long-term cycling stability and appealing rate capability.

1. Introduction

Lithium-ion batteries (LIBs) as a power source and energy storage system become popular and develop fast toward high specific capacities, high current densities and good cycle life. And the key part to develop the lithium-ion batteries is that the preparation of the anode material with fast kinetics of Li-ion insertion/extraction[1, 2]. Recently, three-dimensional (3D) electrodes have attracted more attention for application in LIBs due to their special nature[3]. Meanwhile, the increasing requirements for portable energy storage and the miniaturization of portable electronic devices have led to the rapid development of electrochemical power sources that match the size and energy needs. Three-dimensional microbattery (3D-MB) architecture has been proposed. The 3D electrodes not only has the advantages of the traditional 2D lithium-ion batteries but also can satisfy these new demands[4, 5]. It can effectively tackle the problem of size and energy-density deficiency [6]. Therefore, the 3D electrodes may be the promising field in the development of the new generation of Lithium-ion batteries.

As reported, transition metal oxides have a higher theoretical capacity (ca.500~1000 mA h g^{-1}) than the commercial used anode material---graphite (ca.372 mA h g^{-1})[1, 7]. For instance, Fe$_2$O$_3$, Fe$_3$O$_4$, Co$_3$O$_4$, and MnO$_2$ have attracted a lot of interests as anode materials due to their higher theoretical capacities[1, 8]. Such types of electrode materials are accompanied by the Li-ion insertion/extraction process based on the so-called "conversion reaction", as expressed in Eq. (1)

$$M_xO_y + 2ye^- + 2yLi^+ \longleftrightarrow xM^- + yLi_2O \qquad (1)$$

where M is a transition metal. We can see that, the reaction involves the formation and decomposition of Li$_2$O accompanying the reduction and oxidation of transition metal oxides[9, 10].

Fe$_3$O$_4$ (magnetite) is one of the group of transition metal oxides, which demonstrates the above reactivity mechanism. It has a high initial charge/discharge capacity and a high theoretical capacity around 928 mA h g^{-1} by assuming the reduction of Fe^{3+} and Fe^{2+} to Fe^0 during Li-ion insertion[11, 12]. Furthermore, magnetite also has some other benefits, such as cost-efficiency, environmentally friendliness and relatively high electronic conductivity[8, 13, 14]. However, Fe$_3$O$_4$ has poor cycling stability, poor rate capability and low capacity retention, which limits their widespread use[15, 16]. This may be attributed to the large volume variation during the charge and discharge process, combining the aggregation of the transition metal oxides nanoparticles and the disintegration of the electrode[15]. Therefore, relieving the volume change during the cycles, suppressing the pulverization and of the transition metal oxide material are the effective ways to solve the above defects[17]. Currently, an effective method---preparing nanostructure materials which have potential to meet these demands is commonly used. The reversible capacity of Fe$_3$O$_4$ usually ranges from 350 mA h g^{-1} ~750 mA h g^{-1} when prepared as nanosized powder [18].

After many years of research, lithium-ion batteries(LIBs) anode materials in nanoscale have been investigated and also exhibit a number of unique advantages, such as: (1) short Li-ion transport length due to small particle size; (2) superior accommodation of the strain induced by structure change in active materials; (3) higher charge/discharge rate on account of increased electrode/electrolyte contact proportion; and (4) a higher efficiency of the electron collection owing to the short path lengths for electronic transport[9, 19]. Motivated by these advantages, many reports have exhibited good result about the new anode material. In some papers, the current collector has already been made into nanorod arrays and then packaged with these nanosized active material with high theoretical capacity by electrochemical deposition or hydrothermal reaction[9, 19]. In this paper, in order to combine the advantages of the 3D structure and the nanosized active materials, and then obtain high area

---

a *College of Materials Science and Engineering, Kunming University of Science and Technology, Kunming, 650093, China. E-mail:hanbinganny@163.com*

* *Corresponding author. Tel: +86 10 82338148; Fax: +86 10 82339319. E-mail address: csc@buaa.edu.cn(S. Zhang)*

b *School of Materials Science and Engineering, Beijing University of Aeronautics and Astronautics, Beijing 100191, China*

capacity, we synthesized the 3D nanowire array electrode by template-assisted method, which show high-aspect-ratio and high density[19, 20]. It was expected that more nanoparticles could be deposited and well dispersed on nanowire arrays if we make the nanowire longer and more intense. Actually, the new structure electrodes exhibited high initial capacity, good cycling stability and rate capability than planar electrodes.

2. Experimental

2.1 Fabrication of Cu nanowire arrays as current collectors

The synthesis of Cu nanorod arrays collectors using AAO template has been already reported[9, 19]. And the Cu nanowire arrays collectors were synthesized by the similar method. The high density copper was used as the substrate. The through-hole AAO membrane (the diameter of the pore ranges from 40 to 70 nm) and the cellulose paper separator were clamped in the middle of the two Cu disks (approximately 0.4~0.6 cm^2) using two stainless steel clamps[21]. They were made into a simply equipped battery[19]. Afterwards, the electrodeposition experiments were performed in a three-electrode system (the assembled copper disks served as working electrode and counter electrode respectively, Calomel electrode as reference electrode) and carried out at room temperature using a PARSTAT 2273 electrochemical station. The electrolytic solution contains 200 g/L $CuSO_4 \cdot 5H_2O$ and 90 g/L H_2SO_4. Prior to apply pulse signals, the configuration was immersed into solution and put into vacuum environment to assist impregnation. The deposition of Cu nanowire arrays was based on modulated current pulse signals in the microsecond range after vacuum-assisted impregnation. Pulse 1 is a period of long rest time (0 mA, 250 ms), which is expected to allow the electrode diffuse into the pore of the AAO template, and Pulse 2 is positive pulse (70 mA, 50ms) which was applied to deposit Cu nanowires[21]. After deposition, the samples were dissolved in a 1M NaOH solution for 1h to remove the AAO temple and then rinsed with deionized water for three times, finally, dried in vacuum at 70□.

2.2 Electrodeposition of Fe_3O_4 nanoparticles

The active material of Fe_3O_4 was deposited onto the Cu nanowire arrays by electrodeposition. 2.7 g $FeCl_3 \cdot 6H_2O$ was dissolved in 40 ml alcohol and then 5ml formaldehyde solution was dropt into it. After agitated with magnetic stirring for half an hour, the solution was ageing for 5 hours before using. The prepared solution was diluted to one tenth with deionized water serve as electrolyte. Electrodeposition was also carried out in a three electrode system with a constant voltage of 6V for 1.5 h at room temperature using a direct-current (DC) power. The Cu disks with Cu nanostructure arrays served as cathode, and a graphite sheet served as anode. Meanwhile, Fe_3O_4 was a electrodeposited under the same conditions on mechanically polished planar Cu disks to provide comparison samples[9, 19]. After rinsed with deionized water and dried in the vacuum oven, the samples were annealed at 250℃ for 2 h under N_2 atmosphere.

2.3. Structure analysis and morphology characterization

The phase structure of the resulting 3D nanostructured samples were examined by X-ray diffraction (XRD, Rigaku D/Max-2400) with Cu Kα radiation. Scanning electron microscopy (SEM, Hitachi S-4800), transmission electron microscopy (TEM, JEOL JEM 2010) and field emission transmission electron microscope transmission (FE-TEM, JEOL JEM 2010) were employed to identify the morphology.

2.4. Electrochemical tests

Test cells were assembled in an Ar filled glove box (MB-10-G with TP170b/mono, MBRAUN) using the as-prepared samples (electrode area: 0.6cm^2) as working electrode, lithium sheet as counter reference electrode, and polypropylene film (Celgard-2300) as separator. Electrolyte was 1 M $LiPF_6$ in a mixed solution of ethylene carbonate (EC) and diethyl carbonate (DEC) (1:1 in volume ratio). Each cell was aged for 24 h at room temperature before tests. The galvanostatic measurements were carried out in a battery test system (NEWARE BTS-610, Newware Technology Co., Ltd., China) in a voltage range between 0.02 and 2.5 V (vs. Li/Li^+). Cyclic voltammograms (CVs) were measured with an electrochemical workstation (CHI1100A) at a scanning rate of 0.2 mV s^{-1} between 0.02 and 3 V (vs. Li/Li^+). We choose to report the capacity of these electrodes in μA h cm^{-2}, area being footprint area of the electrode[22].

3. Results and discussion

3.1. Morphology of Cu nanowire array current collector

Fig. 1 (a) and (b) show the plan view and cross-sectional view of Cu nanowires after removing the AAO template. As depicted in Fig. 1 (a), the Cu nanowires uniformly and vertically grow on the copper substrate, which are originated from the microstructure of the AAO template with almost the same pore size. Fig. 1 (b) is the typical SEM images, we can see the diameter of each individual copper nanowire is around 50 nm and the length is more than 4μm which is longer than that reported before. The diameter and length of the nanowires can be controlled by the pore size of template. The obtained current collector with high-aspect-ratio nanowire array structure will be critical to its performance because of the following advantages: (1) the three-dimensional nanowires have a greater specific surface area than the planar Cu disk, so more active materials could be loaded on the surface. (2) the inter-wire distance provides space for the diffusion of electrolyte into the inner region of the electrode, where Li-ions can react with the superficial materials around each nanowire. (3) such space is also helpful for accommodations of the strain caused by the volume variations during cycling[9, 19].

3.2. Morphology of $Cu@Fe_3O_4$ nanostructured electrodes

Fig.1(c) and (d) shows the SEM image of $Cu@Fe_3O_4$ nanowires. We can see that many nanoparticles attach to the surface of the nanowires which are not as smooth as before, and the diameters of nanowires become larger. While, the interspace beween nanowire still exists, so the superiorities of the 3D nanostructure are maintained. Due to the small diameters around 80 nm, Cu nanowires are inclined to agglomerate into thicker nanowire bundles in the process of the electrodeposition of Fe_3O_4, as shown in Fig. 1 (e). Further, when too much active nanoparticles are deposited on them, they tend to form a thin layer on the top of the nanowires as shown in Fig. 1 (f). It is known that the existence of thin layer may aggravate the agglomerate of nanowires, and may give rise to the disintegration of the structure and do harm to the electrochemical characters as reported before[9, 19]. Therefore, we made an effort to obtained high-aspect-ratio nanowires and deposite Fe_3O_4 moderately on nanowires as shown in Fig.1 (c) and (d) to ensure the electrochemical character, by exploring the parameters of electrodeposition. After many attempts, we found 1.5 h may be the best electrodeposition time at the condition of constant voltage. And if the time is longer than it, the layer may be thick. While, if the time is too shorter, there may be no active materials on the nanowires, which result in low capacity.

To confirm the structure of the Cu@Fe_3O_4 nanowire arrays, TEM and FETEM investigation were carried out. We can clearly see the core-shell structure from Fig. 2 (a) and (b). The Cu core is completely coated with a consecutive Fe_3O_4 layer, which is considered to be beneficial for electrochemical performance[15]. The thickness of the Fe_3O_4 nanocrystalline layer is about 30~40 nm and the diameter of the Cu core is approximately 50 nm, which is consistent with the SEM image. The high-resolution TEM (HRTEM) further revealed the structure of Cu@Fe_3O_4 nanowire. The clear lattice structure indicates that the Fe_3O_4 nanolayer is well crystallized, which is resulted from the heat treatment under high temperature. It can be observed from the Fig. 2 (c) that the crystal lattice fringes with spacing of 0.48 nm and 0.29 nm, correspond to the (111) and (220) plane of Fe_3O_4 (The d-spacing = 4.844 Å for the (111) plane and the d-spacing = 2.966 Å for the (220) plane)[13, 14, 23, 24], which are reflected as the initial two peaks in the XRD pattern[25].

3.3. Microstructure study

To clarify the phase of the as-prepared Cu@Fe_3O_4 nanostructured electrodes materials, X-ray diffraction (XRD) measurements were carried out. Fig. 2 (d) shows the typical patterns of the as-prepared sample comparing with simplex Cu. There are two strong peaks at about 43.3◦ and 50.5◦ corresponding to the Cu (111) and the Cu (200) reflections (PDF card no. 03-1005), which is originated from the Cu substrate and the Cu nanowire array. Four weak peaks at about 18.3◦, 30.1◦, 37.0◦, 43.0◦ and 62.5◦ are the typical peaks of Fe_3O_4 (PDF card no. 65-3107)[24]. The (440) peak is stronger than others, suggesting the Fe_3O_4 phase has preferred orientation.

3.4. Electrochemical performance

Half cells using Li foil as both counter and reference electrodes were assembled for the electrochemical measurements. Fig. 3. (a) shows the results of the cyclic voltammograms curves of the half-cell. Cyclic voltammetry (CV) was carried out in the range from 0.02 to 3 V at a scan rate of $0.2 mVs^{-1}$ for 3 cycles. The cathodic peaks at 1.0 and 0.55 V in the 1st sweep starting with an open circuit voltage (OCV, 2.04 V) indicate that the Fe^{3+}/Fe^{2+} converses to Fe^0 and form Li_2O[24, 26]. It has been found that Fe_3O_4 was not directly reduced to Fe^0 during the initial discharge process with the formation of an intermediate phase of $LixFe_3O_4$[15]. The reaction mechanism between Li and Fe_3O_4 can be described with the two steps: (1) $Fe_3O_4+2Li^++2e^- \rightarrow Li_2(Fe_3O_4)$; and (2) $Li_2(Fe_3O_4)+8Li^++8e^- \rightarrow 3Fe+4Li_2O$[2, 24, 25]. In the subsequent two cycles, the two cathodic potential peaks become lower significantly, suggesting the occurrence of some irreversible reactions with the formation of an solid electrolyte interface (SEI) film at the electrode/electrolyte surface due to the reduction of electrolyte in the first cycle[27]. Meanwhile, the cathodic peaks also shift to larger positive potential vs. Li/Li^+ in the subsequent cycles. Particularly, in the second cycle, the peak at 0.55 V shifts to 0.63 V, and the peak at 1.0 V shifts to 1.4 V. This change can assign to electrode polarization[28]. In the anodic scan, the peak at about 1.7 V can be assigned to the oxidation of Fe^0 to Fe^{2+} and Fe^{3+}[29]. In the second and third sweep, the density of the peaks decreased substantially, indicating capacity loss due to the irreversibility of the electrochemical reaction[14, 30].

The discharge/charge curves of the composite at a constant current density of 30 $\mu A\ cm^{-2}$ (the electrode area is about 0.6 cm^2) are presented in Fig 3(b). We can see that, in the initial discharge, the first plateau appears at about 1.3 V, followed by a smooth voltage drop to~0.87 V, corresponding to Li^+ inserting into Fe_3O_4 to form $Li_2Fe_3O_4$[14]. The second extended potential plateau at~0.87 V versus Li/Li^+ reflects the reduction of Fe^{3+}/Fe^{2+} to Fe^0, which is the typical characteristic for Fe_3O_4 based anodes[13, 23]. It shows the lithium storage capacity is 831 $\mu A\ h\ cm^{-2}$ in the first discharge process, the charge capacity is 750 $\mu A\ h\ cm^{-2}$ with no apparent potential plateau in the first charge process[12]. The capacity loss can be ascribed to the irreversible reactions, which is in accordance with the CV curve above. The gap between discharge and charge capacity in the first two cycles is comparatively bigger than the following cycles because the irreversible SEI formation. And the coulombic efficiency of the composite in the following cycles is high (approximately > 94%), which indicates an excellent reversibility of the sample electrode during cycling[31].

Fig 3(c) shows the cycling performances of the Cu@Fe_3O_4 nanowire arrays electrode in a voltage window from 0.02~2.5 V at a current density of 50 $\mu A\ cm^{-2}$ [21, 32]. It can be seen that the discharge capacity of the first discharge is high, and the capacity has a trend of decrease in the initial 10 cycles, while in the following cycles it exhibits a stable capacity of 200 $\mu A\ h\ cm^{-2}$ [22], and the coulombic efficiency increases from 70% to 96% (from the 10 cycle onward)[8]. These changes may be attributed to the high capacity of Fe_3O_4 and the activation process in the initial several charge /discharge cycles. After the activation, both coulombic efficiency and the capacity become stable for 50 cycles[33, 34].

In addition to the improved cycling performance, the Cu@ Fe_3O_4 3D nanowire arrays electrodes also display good rate performance. Fig. 4(a) shows the rate capacities of the composites in a voltage window from 0.05~2.5 V at different current densities. For comparison, the planar Cu@Fe_3O_4 electrodes (with the similar area to 3D electrodes）were also investigated under the same conditions. Obviously, the 3D structured electrodes show enhanced capacity and better cycling stability even at high current density in comparison to the planar one. More specifically, the discharge capacities of the 3D electrode are 206.25, 105.75, 82.75, 62.75 and 97$\mu A\ h\ cm^{-2}$ at current densities of 50$\mu A\ cm^{-2}$, 125 $\mu A\ cm^{-2}$, 250 $\mu A\ cm^{-2}$, 500 $\mu A\ cm^{-2}$, and 50 $\mu A\ cm^{-2}$ respectively[27] (the electrode area is about 0.7 cm^{-2}). The capacity decreases rapidly in the first several circles at current densities of 50μA cm^{-2}, but has no big changes during the current density increases from125 μA cm^{-2} to 500 μA cm^{-2}. Especially, when the current density is set back to 50μA cm^{-2} after 50 cycles, the capacity almost returns back to the initial capacity, suggesting the good rate performance[35, 36]. However, the capacities of planar Cu@Fe_3O_4 electrode at the same current density are all lower than the 3D electrodes. Notablely, the initial capacity of the 3D electrodes is almost 4 times higher. Such superior performance of the 3D electrode could probably be attributed to its high-aspect-ratio nanostructure which has been provided by SEM and TEM[36, 37]. The planar electrodes have smaller specific surface area than the 3D nanostructurede electrodes in the same size, so the amount of active nanoparticles is limited. As we all know the amount of active materials is the main factor to the capacity. Herein, the initial capacity of 3D electrodes is higher markedly. However, we can't expect to enhance the capacity by prolonging the deposition time. If we deposited more nanopaticles on the planar disk, the layer may crack and disintegrate faster, resulting in worse electrical performance. On the contrary, the 3D nanowire array has too large specific surface area to load active naonparticles, contributing to the high initial capacity. The SEM image of the electrodes after cycling can further improve the advantages of the 3D nanostructure. The SEM images of 3D electrode (a) and planar electrode (b) after 100 cycles are shown in the Fig. 5 (a) and (b). In the Fig.5 (a), we can see the Cu@Fe_3O_4 nanowire array still stick on the surface of the Cu substrate, and they almost haven't disintegrated and fall off from the copper but just have some cracks. The inset image also exhibits the magnifying nanowire array. The nanowires still maintain the initial morphology, demonstrating that the structure of 3D nanowire array can release the strain associated with volume changes and keep electrode integrity. This may contribute to the good rate character of the hybrid electrode. On the contrary, the active materials on the planner electrode are aggregated badly and cracks. The comparison between Fig. 5 (a) and (b) can explain why the 3D electrodes have better rate performance than the planar electrodes.

Comparing with the other hybrid electrode, such as TiO_2-B nanowire@a-Fe_2O_3 nanothorn core-branch arrays[38], the microstructure of the Fe_3O_4 3D nanowire arrays electrodes is neoteric, but the specific capacity still needs to be enhanced. This may result from that the TiO_2 could contribute to the capacity more or less. So this maybe a direction in the following study.

4. Conclusions

The Cu@Fe_3O_4 nanowire arrays electrodes were assembled by two-step fabrication process. We used AAO template to grow Cu nanowires with the diameter of 50nm and the length of 4μm onto Cu substrates as nanostructured current collector. The second step was depositing nanosized Fe_3O_4 particles on the surface of the Cu nanowires. The obtained 3D nanowire arrays electrodes were high-aspect-ratio, specifically, the nanowires were long, thin, orderliness, and intense. Simultaneously, the layer of Fe_3O_4 was dense and crystallized well. The initial capacity is almost 4 times higher than the plane electrodes, and it also exhibits a better characteristic of capacity retention even cycled at a high current density. However, the capacity of 3D electrode is not as good as other hybrid electrode with similar microstructure. So this may be the important issue in the following study.

5. Acknowledgement

This work was supported by the National Basic Research Program of China (973 Program) (2013CB934001), National Natural Science Foundation of China (51074011 and 51274017), National 863 Program of China (2012AA052201, and 2012AA110102), and International S&T Cooperation Program of China (2012DFR60530).

6. References

1. X. Zhu, Y. Zhu, S. Murali, M. D. Stollers and R. S. Ruoff, *Acs Nano*, 2011, 5, 3333-3338.
2. C. He, S. Wu, N. Zhao, C. Shi, E. Liu and J. Li, *Acs Nano*, 2013, 7, 4459-4469.
3. D. L. Ma, S. Yuan and Z. Y. Cao, *Chinese Science Bulletin*, 2014, 59, 2017-2023.
4. D. G. Lim, D.-W. Chung, R. Kohler, J. Proell, C. Scherr, W. Pfleging and R. E. Garcia, *Journal Of the Electrochemical Society*, 2014, 161, A302-A307.
5. D. Golodnitsky, M. Nathan, V. Yufit, E. Strauss, K. Freedman, L. Burstein, A. Gladkich and E. Peled, *Solid State Ionics*, 2006, 177, 2811-2819.
6. O. Nilsen, V. Miikkulainen, K. B. Gandrud, E. Ostreng, A. Ruud and H. Fjellvag, *Physica Status Solidi a-Applications And Materials Science*, 2014, 211, 357-367.
7. R. Liu, T. Li, F. D. Han, Y. J. Bai, Y. X. Qi and N. Lun, *Journal Of Alloys And Compounds*, 2014, 597, 30-35.
8. C. Wang, Q. Zhang, Q.-H. Wu, T.-W. Ng, T. Wong, J. Ren, Z. Shi, C.-S. Lee, S.-T. Lee and W. Zhang, *RSC Advances*, 2012, 2, 10680.
9. H. Duan, J. Gnanaraj and J. Liang, *Journal of Power Sources*, 2011, 196, 4779-4784.
10. C. Jiang, E. Hosono and H. Zhou, *Nano Today*, 2006, 1, 28-33.
11. B. Wang, G. Wang, Z. Zheng, H. Wang, J. Bai and J. Bai, *Electrochimica Acta*, 2013, 106, 235-243.
12. M. Hu, Y. Jiang and M. Yan, *Journal Of Alloys And Compounds*, 2014, 582, 563-568.
13. R. Liu, T. Li, F.-D. Han, Y.-J. Bai, Y.-X. Qi and N. Lun, *Journal of Alloys and Compounds*, 2014, 597, 30-35.
14. G. Lu, S. Qiu, J. Liu, X. Wang, C. He and Y.-J. Bai, *Electrochimica Acta*, 2014, 117, 230-238.
15. H. Xia, Y. Wan, G. Yuan, Y. Fu and X. Wang, *Journal of Power Sources*, 2013, 241, 486-493.
16. C. X. Wang, G. J. Shao, Z. P. Ma, S. Liu, W. Song and J. J. Song, *Electrochimica Acta*, 2014, 130, 679-688.
17. Z. P. Zeng, H. L. Zhao, J. Wang, P. P. Lv, T. H. Zhang and Q. Xia, *Journal Of Power Sources*, 2014, 248, 15-21.
18. H. S. Kim, S. H. Baek, M. W. Jang, Y. K. Sun and C. S. Yoon, *Journal Of the Electrochemical Society*, 2012, 159, A325-A329.
19. H. Duan, J. Gnanaraj, X. Chen, B. Li and J. Liang, *Journal Of Power Sources*, 2008, 185, 512-518.
20. N. C. Li, C. R. Martin and B. Scrosati, *Journal Of Power Sources*, 2001, 97-8, 240-243.
21. X. Wu, S. Zhang, L. Wang, Z. Du, H. Fang, Y. Ling and Z. Huang, *Journal of Materials Chemistry*, 2012, 22, 11151.
22. S. Zhang, Y. Xing, T. Jiang, Z. Du, F. Li, L. He and W. Liu, *Journal of Power Sources*, 2011, 196, 6915-6919.
23. Y.-M. Lin, P. R. Abel, A. Heller and C. B. Mullins, *The Journal of Physical Chemistry Letters*, 2011, 2, 2885-2891.
24. Y. Gan, H. Gu, H. Xiao, Y. Xia, X. Tao, H. Huang, J. Du, L. Xu and W. Zhang, *New Journal of Chemistry*, 2014, 38, 2428.
25. Z. Cao and B. Wei, *Journal of Power Sources*, 2013, 241, 330-340.

26. Y. Zou, J. Kan and Y. Wang, *The Journal of Physical Chemistry C*, 2011, 115, 20747-20753.
27. J. Zhao, S. Zhang, W. Liu, Z. Du and H. Fang, *Electrochimica Acta*, 2014, 121, 428-433.
28. L. Yao, X. Hou, S. Hu, J. Wang, M. Li, C. Su, M. O. Tade, Z. Shao and X. Liu, *Journal of Power Sources*, 2014, 258, 305-313.
29. L. Ji, Z. Tan, T. R. Kuykendall, S. Aloni, S. Xun, E. Lin, V. Battaglia and Y. Zhang, *Physical Chemistry Chemical Physics*, 2011, 13, 7139-7146.
30. J. Luo, J. Liu, Z. Zeng, C. F. Ng, L. Ma, H. Zhang, J. Lin, Z. Shen and H. J. Fan, *Nano Letters*, 2013, 13, 6136-6143.
31. J. Qu, Y. X. Yin, Y. Q. Wang, Y. Yan, Y. G. Guo and W. G. Song, *ACS applied materials & interfaces*, 2013, 5, 3932-3936.
32. X. Wu, S. Zhang, H. Fang, Z. Du and R. Lin, *Journal of Power Sources*, 2014, 264, 311-319.
33. X. Zhao, D. Xia and K. Zheng, *ACS applied materials & interfaces*, 2012, 4, 1350-1356.
34. G.-W. Zhou, J. Wang, P. Gao, X. Yang, Y.-S. He, X.-Z. Liao, J. Yang and Z.-F. Ma, *Industrial & Engineering Chemistry Research*, 2013, 52, 1197-1204.
35. S. Zhang, Z. Du, R. Lin, T. Jiang, G. Liu, X. Wu and D. Weng, *Advanced materials*, 2010, 22, 5378-5382.
36. Y. Zhao, J. Li, C. Wu, Y. Ding and L. Guan, *ChemPlusChem*, 2012, 77, 748-751.
37. X. Xu, R. Cao, S. Jeong and J. Cho, *Nano Lett*, 2012, 12, 4988-4991.
38. H. Xia, W. Xiong, C. Lim, K., Q. Yao, F, Y. Wang, D. and J. Xie, P., *Nano Research*, 2014, DOI: 10.1007/s12274-014-0539-3.

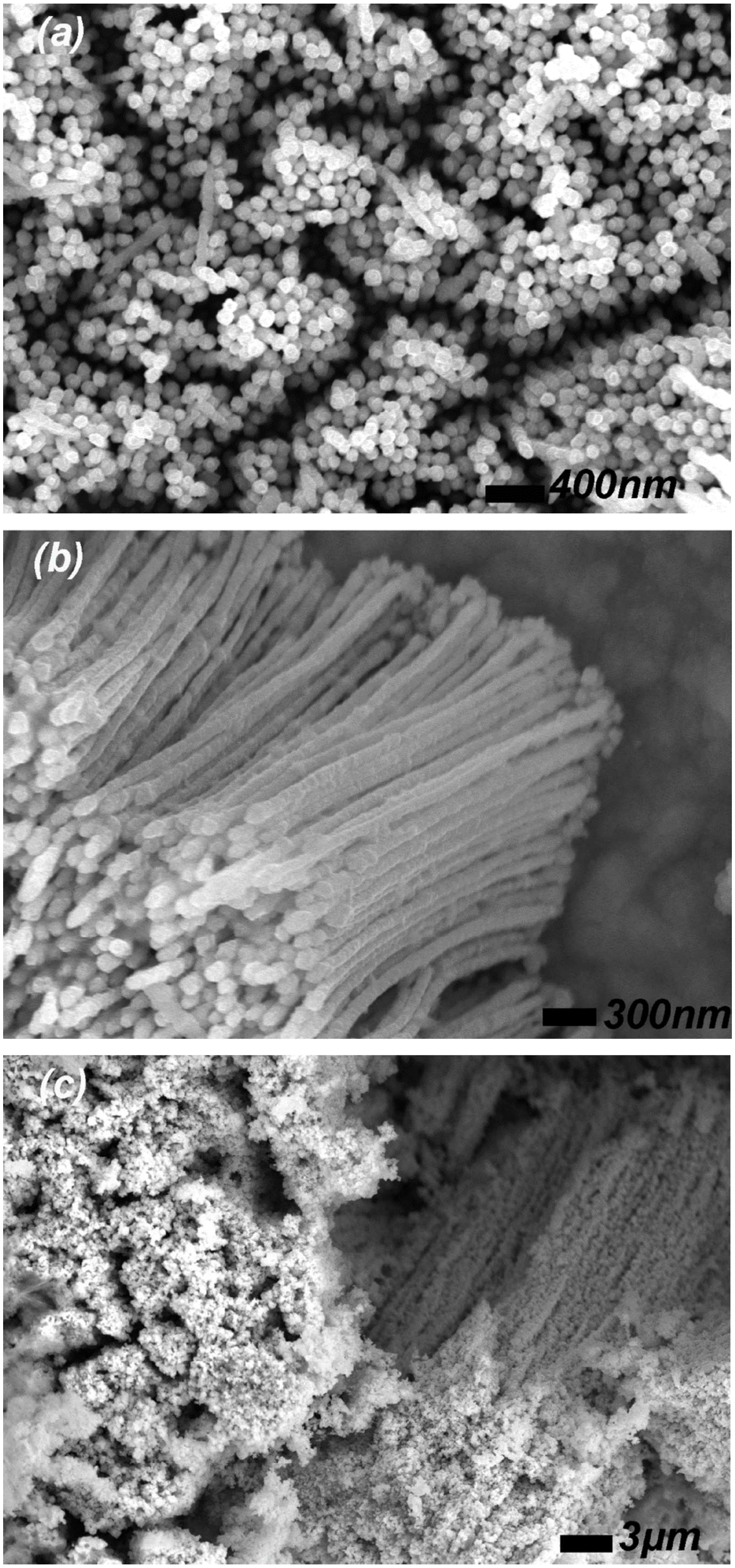
(a)
400nm
(b)
300nm
(c)
3μm

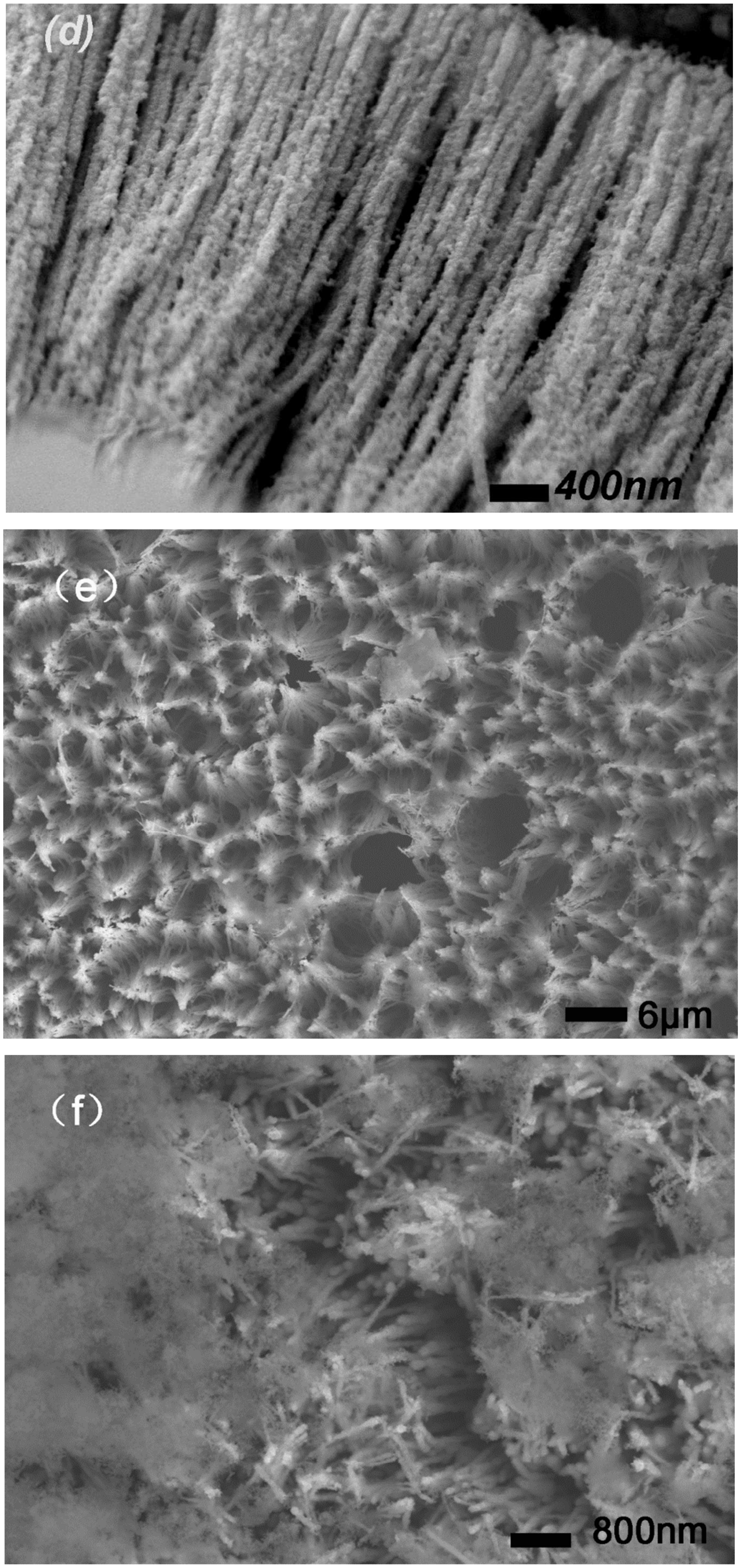

Fig. 1. SEM images of Cu nanowires (a) and the cross-sectional view (b). SEM images of Cu @ Fe_3O_4 nanowires **(c)** and the cross-sectional

view (d). SEM image of nanowire bundles of the Cu@Fe_3O_4 nanowires (e), SEM image of the active materials on the top of the nanowires (f)

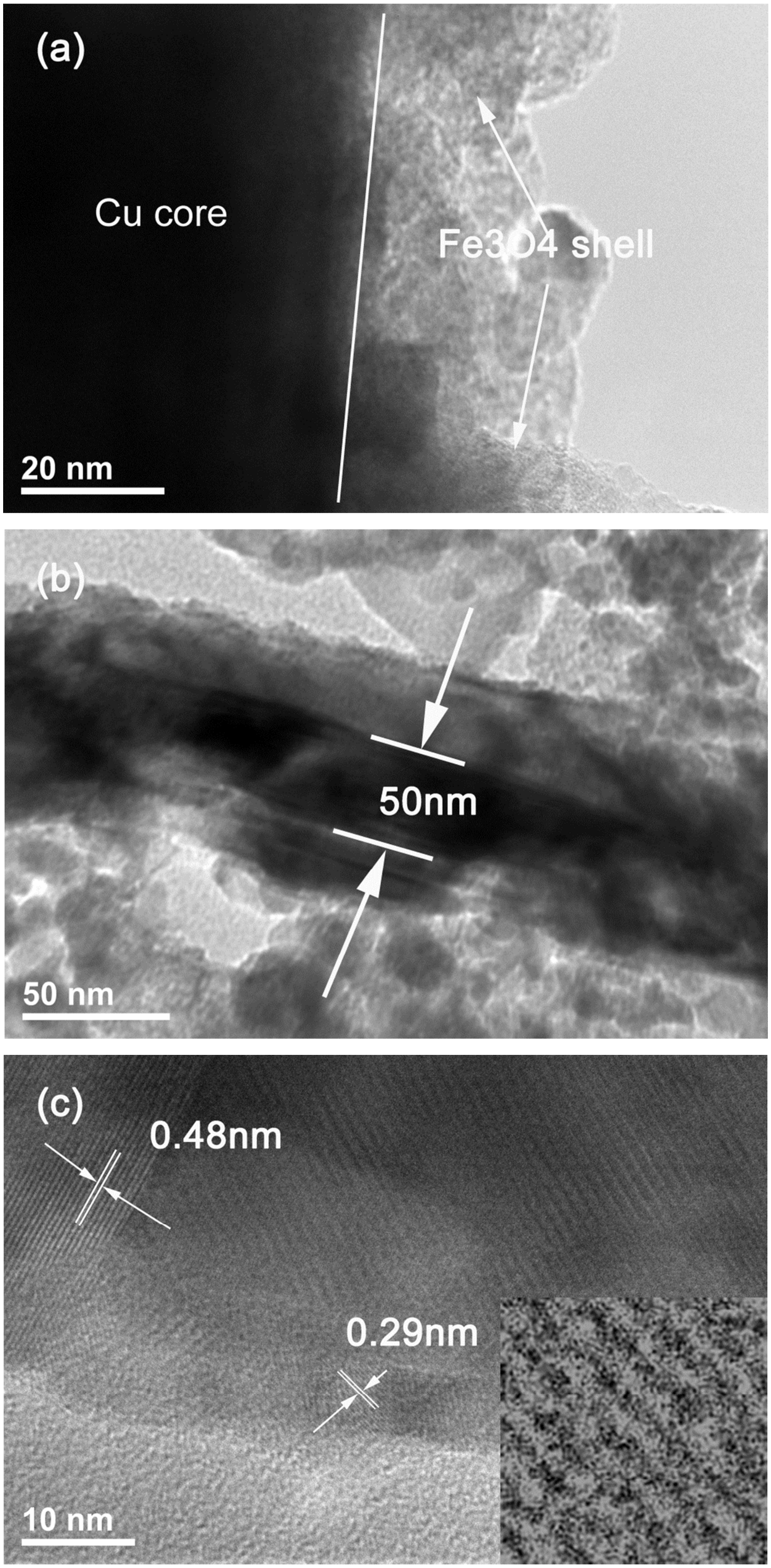

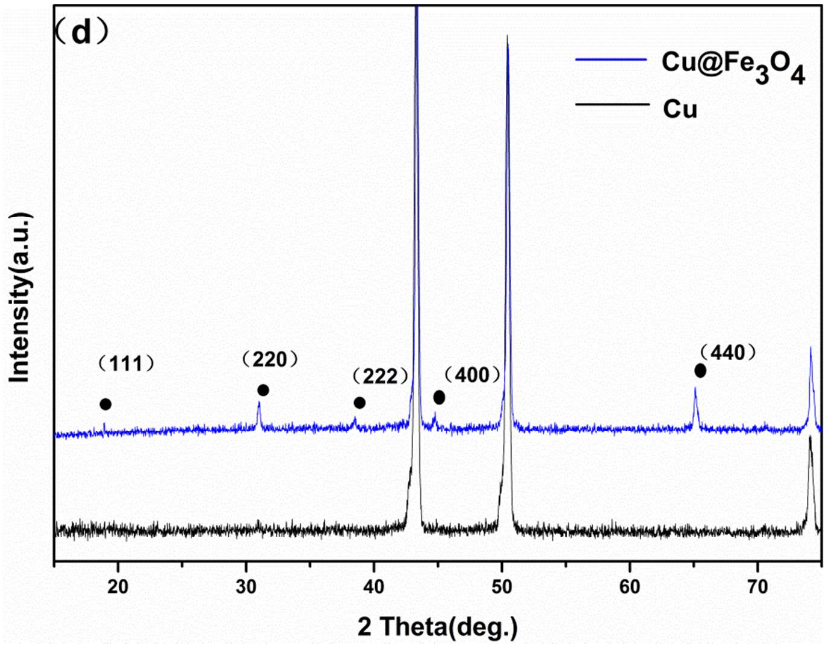

Fig.2 TEM images of individual Cu@Fe$_3$O$_4$ nanowire (a,b), and HRTEM of the Fe3O4 shell (c). (d) XRD of Cu@Fe$_3$O$_4$ compare with the pure Cu.

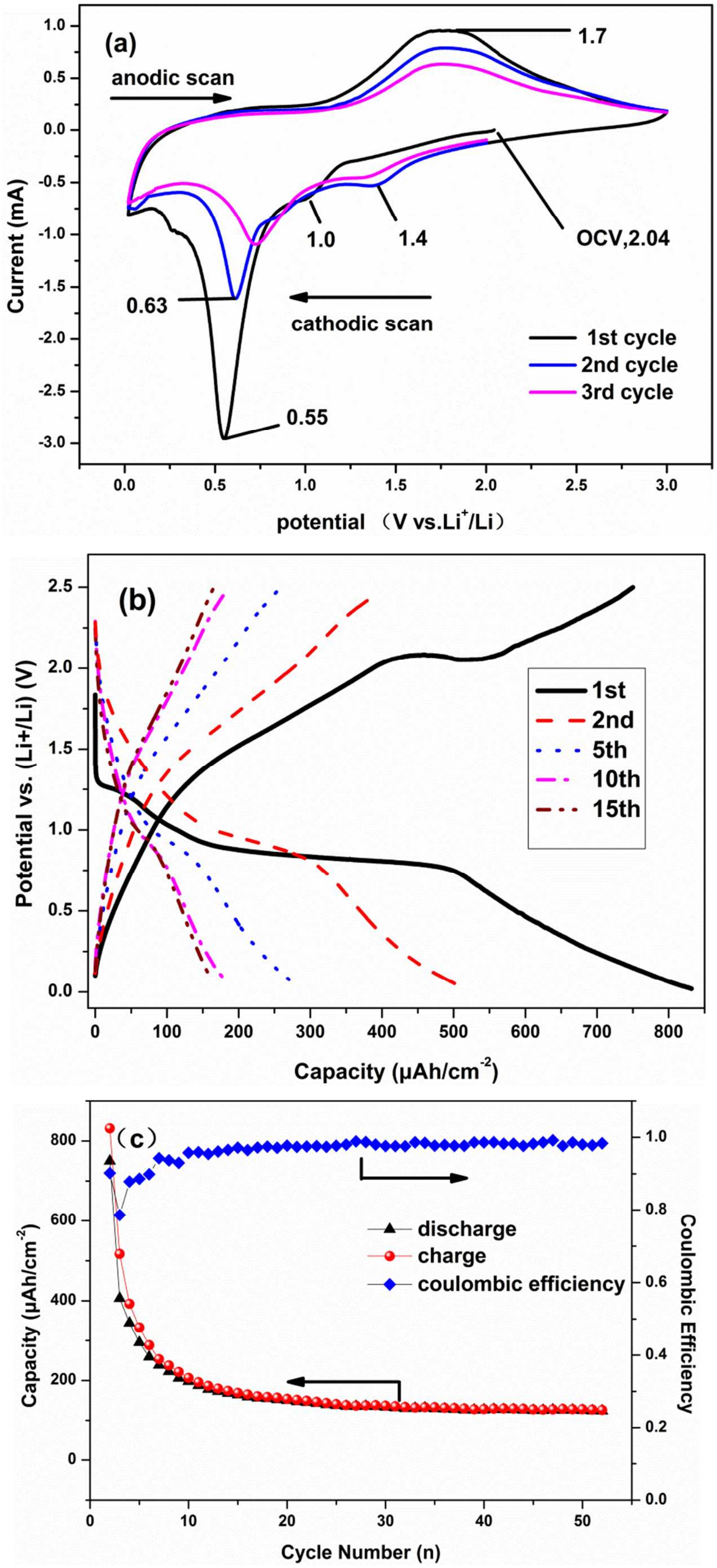

Fig.3. (a) Cyclic voltammograms of Cu@Fe$_3$O$_4$ nanowire electrodes. (b) Charge–discharge curves of the 1st, 2nd, 5th and 10th 20th cycles, and (c) Cycle performances of nano tructured Cu@Fe$_3$O$_4$ and planar Cu electrodes

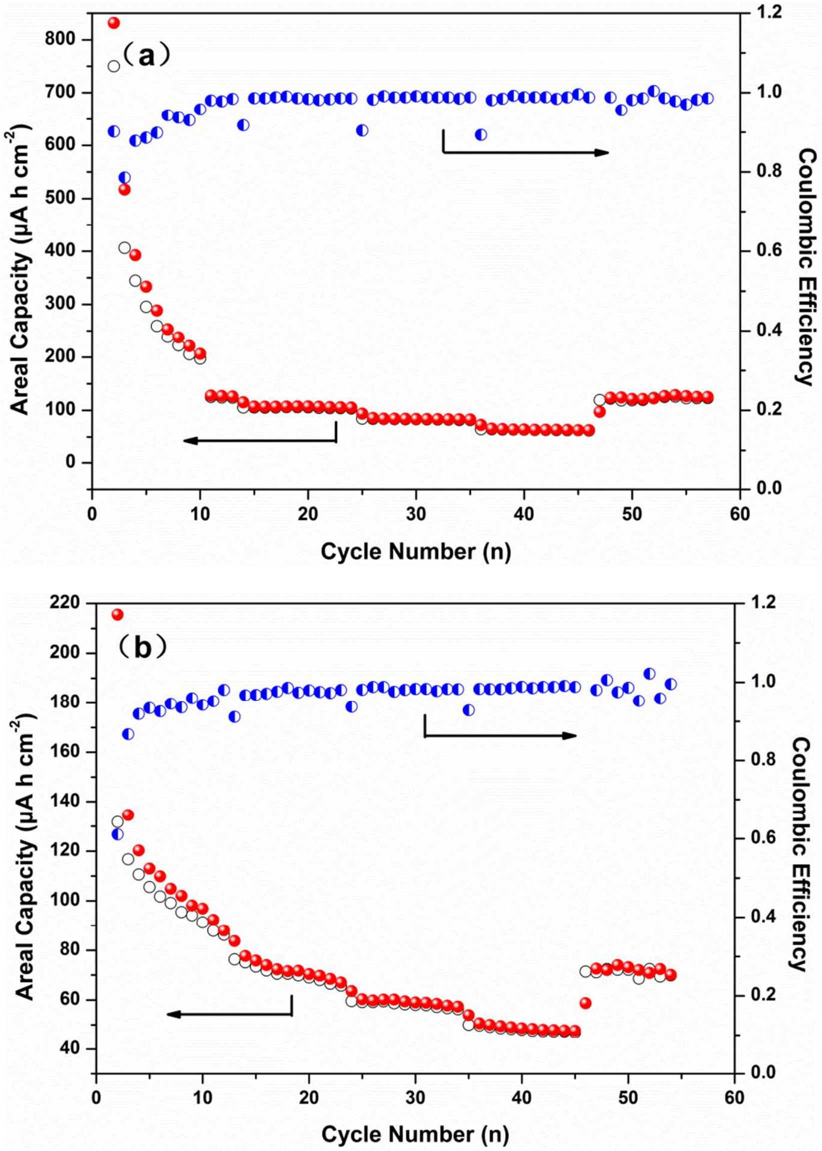

Fig.4. cycling performance of the as-prepared electrodes (a) and planar Cu@Fe_3O_4 electrodes (b) obtained at different rates;

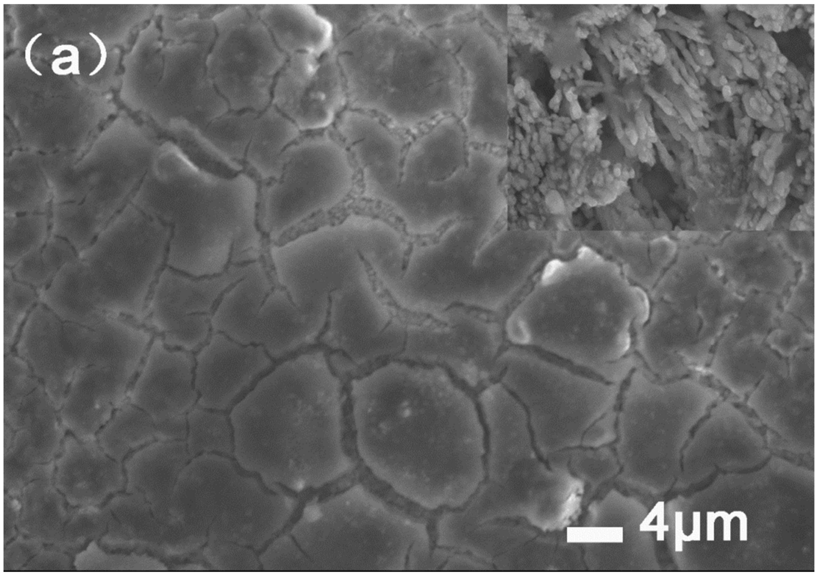

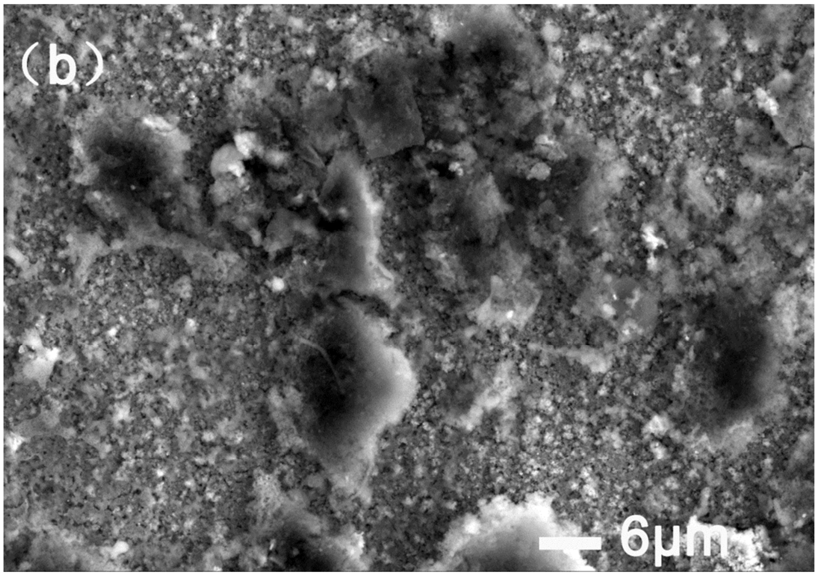

Fig. 5. SEM images of 3D electrode (a) and planar electrode (b) after 100 cycles.